Received: 2 February 2017 | Revised: 18 August 2017 | Accepted: 31 August 2017

DOI: 10.1002/nbm.3836

WILEY NMR IN BIOMEDICINE

RESEARCH ARTICLE

Combined endogenous MR biomarkers to predict basal tumor oxygenation and response to hyperoxic challenge

Thanh-Trang Cao-Pham[1] | Nicolas Joudiou[1] | Matthias Van Hul[2] | Caroline Bouzin[3] | Patrice D. Cani[2] | Bernard Gallez[1] | Bénédicte F. Jordan[1]

[1]Université catholique de Louvain, Louvain Drug Research Institute, Biomedical Magnetic Resonance Research Group, Brussels, Belgium

[2]Université catholique de Louvain, Louvain Drug Research Institute, Metabolism and Nutrition Research Group, Brussels, Belgium

[3]Université catholique de Louvain, IREC Imaging Platform, Brussels, Belgium

Correspondence
B. F. Jordan, Biomedical Magnetic Resonance Group (REMA), Louvain Drug Research Institute, Université catholique de Louvain, Avenue Mounier 73 – B1.73.08, B-1200 Brussels, Belgium.
Email: benedicte.jordan@uclouvain.be

Funding information
Fournier-Majoie Foundation; Belgian National Fund for Scientific Research (FNRS)

Hypoxia is a common feature of solid tumors, which translates into increased angiogenesis, malignant phenotype cell selection, change in gene expression and greater resistance to radiotherapy and chemotherapy. Therefore, there is a need for markers of hypoxia to stratify patients, in order to personalize treatment to improve therapeutic outcome. However, no modality has yet been validated for the screening of hypoxia in routine clinical practice. Magnetic resonance imaging (MRI) R_1 and R_2^* relaxation parameters are sensitive to tissue oxygenation: R_1 is sensitive to dissolved oxygen and R_2^* is sensitive to intravascular deoxyhemoglobin content. Two rat tumor models with distinct levels of hypoxia, 9L–glioma and rhabdomyosarcoma, were imaged for R_1 and R_2^* under air and carbogen (95% O_2 and 5% CO_2) breathing conditions. It was observed that the basal tumor oxygenation level had an impact on the amplitude of response to carbogen in the vascular compartment (R_2^*), but not in the tissue compartment (R_1). In addition, the change in tissue oxygenation estimated by ΔR_1 correlated with the change in vascular oxygenation estimated by ΔR_2^*, which is consistent with an increase in oxygen supply generating an elevated tumor pO_2. At the intra-tumoral level, we identified four types of voxel to which a hypoxic feature was attributed (mild hypoxia, severe hypoxia, normoxia and vascular steal), depending on the carbogen-induced change in R_1 and R_2^* values for each voxel. The results showed that 9L–gliomas present more normoxic fractions, whereas rhabdomyosarcomas present more hypoxic fractions, which is in accordance with a previous study using ^{18}F–fluoroazomycin arabinoside (^{18}F–FAZA) and electron paramagnetic resonance (EPR) oximetry. The response of the combined endogenous MRI contrasts to carbogen challenge could be a useful tool to predict different tumor hypoxic fractions.

KEYWORDS

ΔR_1, ΔR_2^*, carbogen, MRI, tumor hypoxia

1 | INTRODUCTION

Hypoxia is a micro-environmental component of solid tumors and an important prognostic biomarker for tumor aggressiveness and patient outcome. This feature is related to the recurrence of tumors and the failure of cancer treatment. In a systematic review of over 10 000 patients, Overgaard[1] found that the modification of tumor hypoxia improves the efficiency of radiotherapy. Modalities are under evaluation in an effort to counteract the negative effects of hypoxia.[2] Regrettably, screening for the presence of hypoxia is not an entry criterion prior to hypoxia modification in trials.[2] To bridge the gap between the prevalence of tumor hypoxia and clinical routine practice, there is a need to identify

Abbreviations used: BOLD, blood oxygenation level-dependent; BSA, bovine serum albumin; BW, bandwidth; CB, carbogen; DAB, 3,3′-diaminobenzidine; DCE, dynamic contrast-enhanced; dHb, deoxyhemoglobin; EPR, electron paramagnetic resonance; FA, flip angle; ^{18}F–FAZA, ^{18}F–fluoroazomycin arabinoside; FOV, field of view; IR-FISP, inversion-recovery fast imaging with steady state precession; MOBILE, mapping of oxygen by imaging lipids relaxation enhancement; MRI, magnetic resonance imaging; PISTOL, proton imaging of siloxanes to map tissue oxygenation levels; RARE, rapid acquisition with relaxation enhancement; ROI, region of interest; RPMI, Roswell Park Memorial Institute; SEM, standard error of the mean; SSFP-FID, Steady State Free Precession Free Induction Decay; TBS, Tris- Buffered Saline; Tris/EDTA, tris(hydroxymethyl)aminomethane/ethylenediaminetetraacetic acid; α-SMA, α-smooth muscle actin

markers of hypoxia in order to stratify patients who might benefit from oxygen modulation and to tailor therapy to the characteristics of the tumor. Several techniques allow the quantification of tumor oxygenation,[3,4] e.g. ^{19}F–magnetic resonance imaging (^{19}F–MRI) of perfluorocarbon,[5] electron paramagnetic resonance (EPR) oximetry,[6] ^{1}H–MRI of hexamethyldisiloxane PISTOL (proton imaging of siloxanes to map tissue oxygenation levels),[7] polarographic needle electrodes[8] and fiberoptic probes.[9] Nevertheless, these methods are either invasive or require the injection of a reporter probe.

The oxygen-sensitive endogenous MRI contrasts, R_1 and R_2^*, are considered to be potential methods for the evaluation of tumor hypoxia. The effective spin–spin relaxation rate R_2^* is sensitive to the concentration of deoxyhemoglobin (dHb) per volume of tissue. A decrease in [dHb], e.g. an increase in blood saturation, results in a decrease in R_2^*. However, R_2^* is not only sensitive to the change in blood oxygenation through the change in [dHb], but is also sensitive to factors unrelated to the change in oxygenation, such as hematocrit, vascular volume, pH, flow and vessel density,[10] as well as the experimental setting, e.g. voxel size, shimming procedure, TE sampling and quantification method.[11]

The spin–lattice relaxation rate R_1 is sensitive to the oxygen molecules dissolved in plasma and tissue fluid. Nevertheless, the change in relaxivity constant as a function of O_2 depends on the dissolved media.[12] Thus, R_1 is biased by factors independent of the change in O_2 content, such as the water content of tissue or the blood flow.[12] In 2013, Jordan et al.[13] developed a noninvasive R_1-based MRI method to measure tumor oxygenation. The method with the acronym MOBILE (mapping of oxygen by imaging lipids relaxation enhancement) explores the signal of R_1 in lipids instead of the global R_1, as the solubility of oxygen in lipids is higher than that in water. It was shown in lipid-rich mammary tumors that lipid R_1 was more sensitive to the change in tumor oxygenation than the conventional global R_1.[14] Because this method is not applicable in tumors with a low lipid content, we have recently proposed a method in which the global R_1 signal is deconvoluted into fast and slow components attributed to lipid and water relaxation, respectively.[15]

As R_1 and R_2^* reflect different properties of tumor oxygenation, the combination of these two parameters provides complementary information which can aid in the interpretation of MRI data.[16] Previous studies using R_1 and R_2^* have been performed on animals,[17-21] as well as on humans,[16,22] to obtain insights into tissue oxygenation. However, these studies used mean values of R_1 and R_2^*, and did not take into account the tumor heterogeneity and the extent of hypoxia, which are crucial factors for the stratification of patients. In the work of Remmele et al.,[22] the scatter plots of ΔR_1 and ΔR_2^* were employed to investigate the response of different regions of interest to carbogen (CB) breathing. O'Connor et al.[23] demonstrated that the combined information on the oxy-R fraction (fraction lacking a positive ΔR_1 in response to oxygen challenge) and perfusion data, measured by dynamic contrast-enhanced (DCE)-MRI, was correlated with the hypoxic fraction detected by pimonidazole in two different vascularized tumor models, 786–0-R and SW620.

The breathing of hyperoxic gas is a simple method to improve tumor oxygenation. Yet, the response varies between individuals and within tumors. The purpose of this work was to study the role of the basal tissue and vascular tumor oxygenation on the amplitude of response to CB challenge (95% O_2 and 5% CO_2) at the inter-tumoral level, using the combined parameters R_2^* and three types of R_1 (global R_1 or R_{1G}, water R_1 or R_{1W}, lipid R_1 or R_{1L}). The analysis of the intra-tumoral level allowed the categorization of voxels into four types to which a hypoxic feature was attributed (mild hypoxia, severe hypoxia, normoxia, vascular steal). We aimed to compare R_{1G}, R_{1W} and R_{1L} in terms of their sensitivity and predictive power to evaluate the response of a tumor to CB breathing. Two rat tumor models, rhabdomyosarcoma and 9L–glioma, exhibiting distinct basal oxygenation status and different levels of response to CB breathing, were used. The rhabdomyosarcoma model has been described previously to be more hypoxic and less responsive to CB breathing than the 9L–glioma model.[24] Indeed, the mean pO_2 values recorded by EPR oximetry were 9 ± 1 mmHg and 5 ± 1 mmHg at baseline, and increased to 17 ± 2 mmHg and 9 ± 1 mmHg under CB breathing, for 9L–gliomas and rhabdomyosarcomas, respectively.[24] It should be noted that 10 mmHg is often suggested as the radiosensitivity threshold. The 9L–glioma model was therefore more responsive to CB by increasing the pO_2 value above this threshold.

2 | MATERIALS AND METHODS

The study was approved by the local ethics committee. The study was undertaken in accordance with the national and local regulations of the ethical committee (agreement number UCL/2014/MD/026).

2.1 | Tumor models

Two tumor models were included in the study: rhabdomyosarcoma (n = 29) and 9L–glioma (n = 25).

Fragments from a syngeneic rhabdomyosarcoma (1 mm^3) were grafted subcutaneously into the thigh of male adult WAG/Rij rats, according to a model developed by the Laboratory of Experimental Radiobiology, Katholieke Universiteit Leuven, Belgium.

9L–glioma cells were grown in Roswell Park Memorial Institute (RPMI) medium supplemented with 10% fetal calf serum (heat inactivated), 1% of a mixture of antibiotics (penicillin, 100 UI/mL; streptomycin, 0.1 mg/mL), 1% nonessential amino acids and 1% sodium pyruvate. Cells were maintained in a balanced wet atmosphere (37°C and 5% CO_2). To establish 9L–glioma tumors *in vivo*, male adult Fisher F344 rats were inoculated subcutaneously in the thigh with 5×10^6 cells.

Tumor implantations were performed under general anesthesia with intraperitoneal injection of ketamine and xylazine (80 and 10 mg/kg, respectively) in rats weighing between 200 and 250 g. The animals were introduced into the study when the tumors reached 15–20 mm.

2.2 | Experimental design

Two cohorts were involved. The MR measurements were performed on the first cohort including 22 rhabdomyosarcomas and 18 9L–gliomas.

The second cohort included seven rhabdomyosarcomas and seven 9L–gliomas. Animals of the second cohort were euthanized using an overdose of pentobarbital when the tumors reached 15–20 mm. Tumors were harvested and cut in half. One half was dedicated to the measurement of the lipid content. Immunohistochemistry was performed on the other half of the tumor to quantify the mature blood vessels.

2.3 | MR measurements

Animals of the first cohort were subjected to R_1 and R_2^* measurements under baseline (air breathing) and hyperoxic (after 30 min of CB inhalation) conditions (Supporting Information Figure S1). Rats were anesthetized with isoflurane 1.5% during MRI experiments. Gas delivery (medical air or CB mixed with isoflurane) was continuous at 2 L/min through a nosepiece.

MRI was performed on an 11.7-T, 16-cm inner-diameter bore system (Bruker, Biospec, Ettlingen, Karlsruhe, Germany) with a 7-cm birdcage coil for signal transmission and a surface coil for signal reception. A warm water blanket was used to maintain the animal's temperature at 37°C, and the temperature was monitored with an MR-compatible rectal probe.

A multi-slice rapid acquisition with relaxation enhancement (RARE) sequence was first used to determine the most representative tumor slice for further measurement, with the following parameters: TE/TR/RARE-factor/field of view (FOV)/matrix size/slice thickness = 10.66 ms/2500 ms/6/35 × 35 mm^2/256 × 256/1 mm. The segmented inversion-recovery fast imaging with steady state precession (IR-FISP) sequence (SSFP-FID or Steady State Free Precession Free Induction Decay mode) was used for R_1 acquisition with the following parameters: TR/TE/flip angle (FA)/bandwidth (BW)/FOV/matrix size/slice thickness = 4 ms/1.35 ms/10°/100 kHz/55 × 30 mm^2/100 × 85/1 mm, four segments, 100 TI from 13 ms to 8329 ms every 84 ms, and a total acquisition time of 20 min. The resonance frequency for excitation of the R_1 sequence was on resonance for water. Multi-gradient echo R_2^* images were acquired at TR/FA/slice thickness = 3000 ms/15°/1 mm, with a FOV of 35 × 35 mm^2 on a 256 × 256 matrix, with 12 echoes from 3.5 ms to 58.5 ms every 5 ms. The total acquisition time was 9 min and 36 s.

2.4 | Dosage of total lipids

The total lipid content of the tumor was measured by gravimetry following the Folch extraction method with slight modifications. We extracted lipids from about 100 mg of tumor tissue. The sample (M) was homogenized with 1 mL of Folch solution (methanol–chloroform, 1: 2) by a TissueLyser (Qiagen, Hilden, Germany) for 8 min at 30 Hz. The homogenate was centrifuged at 1006g for 5 min to separate the solid and liquid phases. The liquid (lipid) phase was collected in the first centrifuge tube. The pellet was then extracted twice with 1 mL of Folch solution each time. The homogenates were collected in the second centrifuge tube and mixed at room temperature for 20 min. A solution of 0.9% NaCl was added to the two centrifuge tubes (0.2 volume of the lipid phase). The mixtures were then vortexed twice for 1 min each time and centrifuged at 931g for 10 min. The lower chloroform phases in the two tubes were transferred into a preweighed vial (W_{pre}). The vial was dried under a continuous nitrogen flow until a constant mass was achieved (W_{post}). The percentage dry mass of lipids (% lipids) was calculated as:

$$\%\,\text{lipids} = \frac{W_{post} - W_{pre}}{M} \times 100$$

2.5 | Histological analysis for pericyte coverage

Tumors were formalin-fixed and paraffin-embedded. α-Smooth muscle actin (α-SMA) staining was performed on 5-μm sections to detect mature blood vessels covered by pericytes. After manual deparaffinization, endogenous peroxidases were inhibited by a 20-min treatment with 3% H_2O_2 in methanol. Sections were then subjected to antigen retrieval in tris(hydroxymethyl)aminomethane/ethylenediaminetetraacetic acid (Tris/EDTA) buffer, pH 9, at 98°C for 45 min, and then at room temperature for 15 min with 540 μL of Triton 20% added. Aspecific antigen-binding sites were blocked with a Tris-Buffered Saline (TBS) solution containing 5% bovine serum albumin (BSA) and 0.05% Triton. Slices were stained with mouse anti-human α-SMA primary antibodies (Dako M0851, Agilent Technologies Belgium, Diegem, Belgium) overnight at 4°C at a 1: 500 dilution, followed by incubation with envision anti-mouse secondary antibodies (Dako K4001) for 30 min at room temperature. This reaction was visualized using 3,3′-diaminobenzidine (DAB) (Dako K3468). After counterstaining with hematoxylin (Dako S3301), slices were dehydrated and coverslipped.

Slides were finally digitalized at 20× magnification with an SCN400 slide scanner (Leica, Wetzlar, Germany). Images were analyzed using Tissue IA software (Leica Biosystems, Dublin, Ireland). Color deconvolution was applied to each pixel using hematoxylin and DAB matrices of the software. On the DAB matrices, a threshold was adjusted for DAB detection according to intensity (gray values from 0 to 255). The results were expressed as α-SMA-positive area percentages and calculated as (α-SMA-stained area/total tissue area) × 100.

2.6 | Data analysis and statistics

Data analysis was performed using an in-house program developed under ImageJ and MATLAB (MATLAB R2013b, The Math Works, Massachusetts, United States). R_1 and R_2^* maps were calculated with an MRI analysis calculator plug-in in ImageJ software. This MRI analysis method is adapted from the original plugin created by Karl Schmidt (http://rsb.info.nih.gov/ij/) using a curve-fitting method based on the Simplex technique. R_{1L} and R_{1W} were extracted from the R_{1G} map by a biexponential deconvolution method. Hence, the term R_{1G} refers to R_1 acquired by MRI and is the sum of the contributions of R_{1W} and R_{1L}. Meanwhile, R_{1L} and R_{1W} indicate the generated data obtained by the deconvolution of R_{1G}. Regions of interest (ROIs) were drawn manually around the tumor on the selected anatomical slice and were transferred to R_{1L}, R_{1W}, R_{1G} and R_2^* maps of the same slice. The subtraction of the two maps acquired under air and CB breathing conditions was performed voxel by voxel, resulting in maps of ΔR_{1L}, ΔR_{1W}, ΔR_{1G} and ΔR_2^*. Co-registration was performed using a homemade script on Matlab. During acquisition, a similar orientation was used for the R_2^* and R_1 maps so that only translation transformations were needed for co-registration.

For the multi-parametric analysis, the spatial resolution of the R_{1L}, R_{1W} and R_{1G} maps was adapted to the size of the voxel of the R_2^* maps. After obtaining the delta maps, we superimposed the two maps of ΔR_{1L} (or ΔR_{1W} or ΔR_{1G}) and ΔR_2^* voxel by voxel by selecting a common point to navigate. We established for each tumor a scatter plot of CB-induced ΔR_2^*, ΔR_1. Each voxel was presented by a point in the scatter plot (ΔR_2^*, ΔR_1). The point was then encoded with a color code, based on the position over the four quadrants of the scatter plot. Blue was dedicated to voxels with $\Delta R_1 > 0$ and $\Delta R_2^* \geq 0$, cyan to voxels with $\Delta R_2^* > 0$ and $\Delta R_1 < 0$, orange to voxels with $\Delta R_1 \leq 0$ and $\Delta R_2^* < 0$, and red to voxels with $\Delta R_1 > 0$ and $\Delta R_2^* < 0$. The number of voxels was calculated and the percentage was generated for each color in a tumor.

It should be noted that there was no significant difference in the number of voxels analyzed between the two models. The numbers of voxels analyzed per tumor were 5435 ± 403 and 5927 ± 322 for 9L–gliomas and rhabdomyosarcomas, respectively (p = 0.34, Student's t-test).

For Figures 1-3, we fitted the mean value of the ROI. For Figure 4, tumors were analyzed voxel-wise. The ΔR_1 map was superimposed on the ΔR_2^* map and the percentages of the four types of voxel were obtained for each tumor. Figure 4 features the mean value of each type of voxel of the tumors in the same models.

Statistical analyses were performed with the GraphPad (Prism) program (GraphPad Software, Inc., California, United States). Results were expressed as mean ± standard error of the mean (SEM) (Table 1). To evaluate the differences between groups of data, we used the unpaired t-test (Table 1). The linear associations between R_2^* and ΔR_2^* (Figure 1), between ΔR_2^* and ΔR_{1L}, ΔR_2^* and ΔR_{1W}, and ΔR_2^* and ΔR_{1G} (Figure 2), and

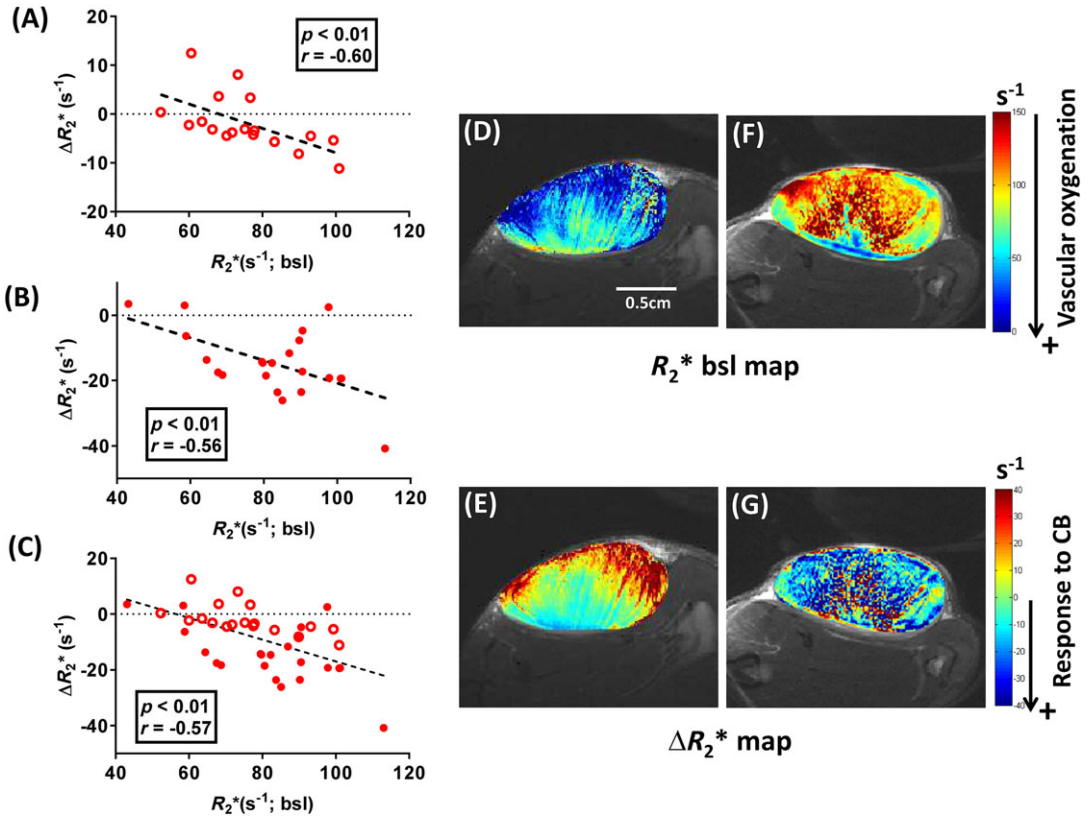

FIGURE 1 (A–C) Correlation between the median values of baseline (bsl) R_2^* and carbogen (CB)-induced ΔR_2^* for 9L-gliomas (A), rhabdomyosarcomas (B) and the pooled data (C). Each point represents one individual tumor. (D) Representative parametric maps showing the R_2^* baseline of a rhabdomyosarcoma. (E) Representative parametric maps showing ΔR_2^* of a rhabdomyosarcoma. (F) Representative parametric maps showing the R_2^* baseline of a 9L–glioma. (G) Representative parametric maps showing ΔR_2^* of a 9L–glioma. ΔR_2^* was obtained by subtracting R_2^* baseline from R_2^* CB. Areas in which $\Delta R_2^* < 0$ are expected to show a decrease in deoxyhemoglobin content [dHb]

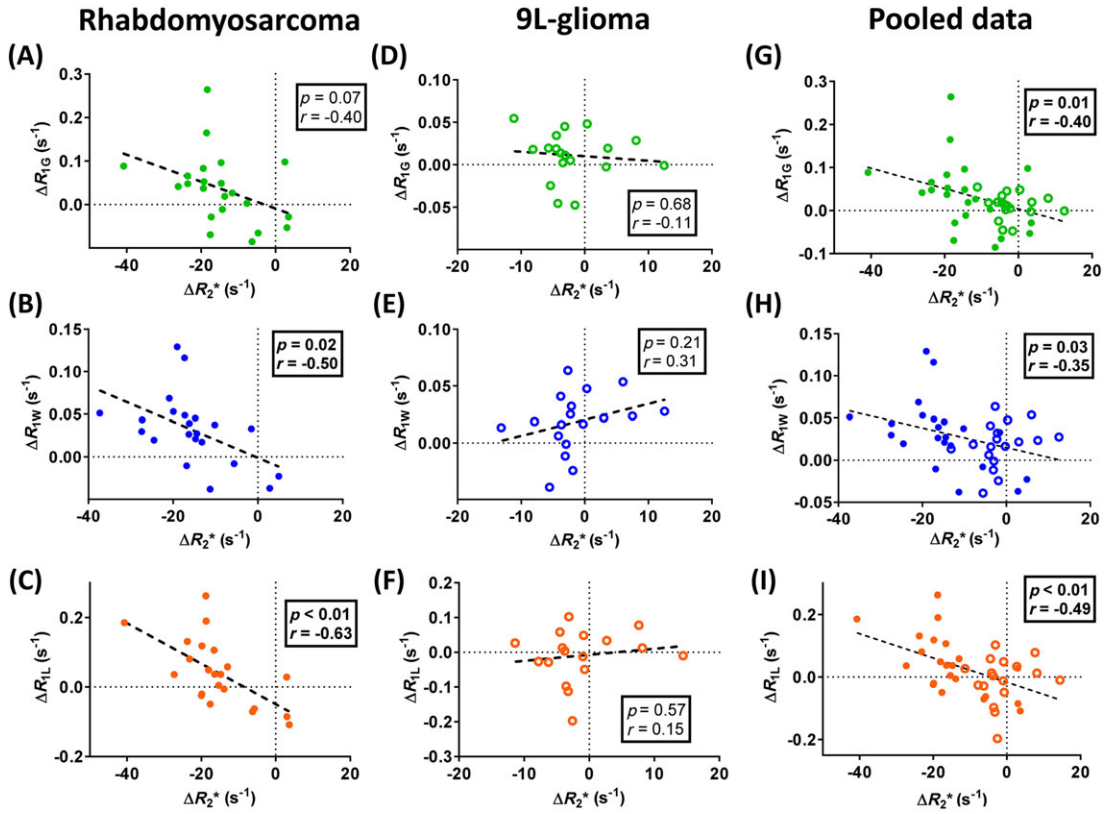

FIGURE 2 Correlations between the median values of ΔR_{1G}, ΔR_{1W}, ΔR_{1L} and ΔR_2^* for rhabdomyosarcomas (A–C), 9L–gliomas (D–F) and the pooled data (G–I). Graphs show correlations between ΔR_2^* and ΔR_{1G} (A, D, G), ΔR_{1W} (B, E, H) and ΔR_{1L} (C, F, I) in response to carbogen (CB) challenge. Each point represents one individual tumor

between R_{1G} and ΔR_{1G}, R_{1L} and ΔR_{1L}, and R_{1W} and ΔR_{1W} (Figure 3) were tested by correlation analysis. For all tests, $p < 0.05$ was considered to be significant.

3 | RESULTS

3.1 | In the vascular compartment, the basal tumor oxygenation influences the amplitude of response to a hyperoxic challenge

As R_2^* is sensitive to the intravascular [dHb], we decided to examine whether the amplitude of change induced by the hyperoxic challenge in the tumor vascular oxygenation was influenced by its basal status.

An increase in vascular oxygenation converts dHb to HbO_2 and thus results in a decrease in R_2^*. It should be noted that the level of hemoglobin saturation at baseline, estimated by the basal R_2^*, can also influence the tumor response to the hyperoxic gas challenge.[21] We observed strong correlations between ΔR_2^* and basal R_2^* (Figure 1A: 9L-glioma, $p < 0.01$ and $r = -0.60$; Figure 1B: rhabdomyosarcoma, $p < 0.01$ and $r = -0.56$; Figure 1C: pooled data, $p < 0.01$ and $r = -0.57$), meaning that tumors that had a better basal vascular oxygenation status (slow basal median R_2^*) were less responsive to CB breathing than tumors that had a lower basal vascular oxygenation status (fast basal median R_2^*). No significant differences were observed between basal R_2^* of 9L–glioma (75.56 ± 3.20 s^{-1}) and basal R_2^* of rhabdomyosarcoma (82.29 ± 3.55 s^{-1}) ($p = 0.18$).

This observation is also true at the intra-tumoral level. Figure 1D–G shows representative maps of R_2^* and CB-induced ΔR_2^* of the two tumor models. In the R_2^* basal map (Figure 1D, F), the tumor periphery (colder color) has a better vascular oxygenation than the tumor core (hotter color). Meanwhile, the ΔR_2^* maps (Figure 1E, G) show that the tumor core, which has a lower basal vascular oxygenation, responds better to CB (colder color), and that the tumor periphery, which has a better basal vascular oxygenation, responds less well to CB (hotter color). Significant correlations between R_2^* and ΔR_2^* of voxels within the two presented tumors were also observed (Supporting Information Figure S2A: $p < 0.01$, $r = -0.62$ for the presented rhabdomyosarcoma; Figure S2B: $p < 0.01$, $r = -0.65$ for the presented 9L–glioma), meaning that voxels that had a better basal vascular oxygenation status (slow basal R_2^*) were less responsive to CB breathing than were voxels that had a lower basal vascular oxygenation status (fast basal R_2^*). It should be noted that a higher R_2^* could be associated with the accumulation of the paramagnetic debris of necrosis. This possibility was excluded as no necrosis was detected by histology at this stage of development (15–20 mm).

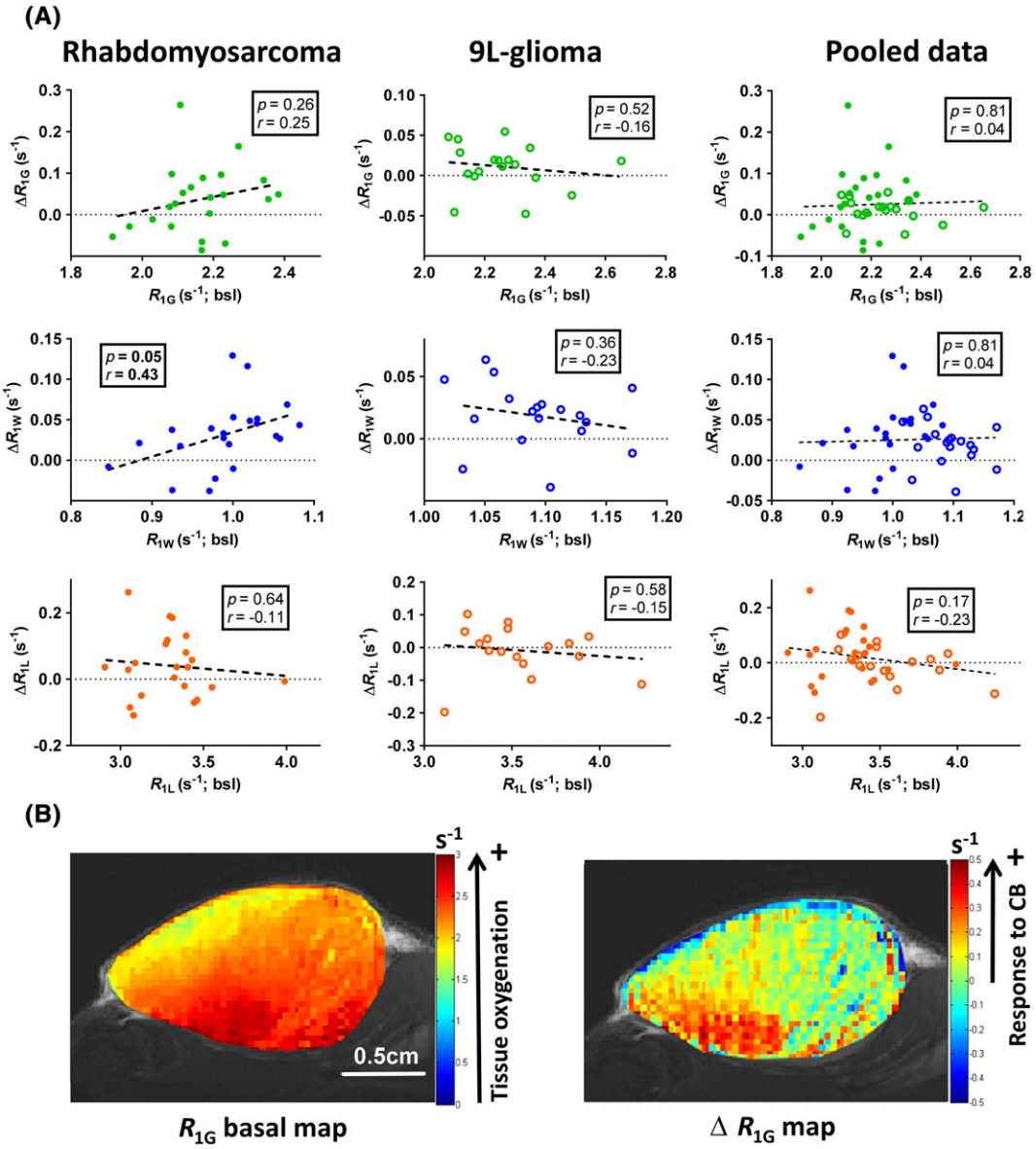

FIGURE 3 (A) Correlations between the median values of ΔR_{1G} and basal R_{1G} (first row), ΔR_{1W} and basal R_{1W} (second row), and ΔR_{1L} and basal R_{1L} (third row) for rhabdomyosarcoma (left column), 9L–glioma (middle column) and the pooled data (right column). Each point represents one individual tumor. (B) Representative parametric maps showing R_{1G} baseline (bsl) (left) and carbogen (CB)-induced ΔR_{1G} (right) of a rhabdomyosarcoma

3.2 | A change in vascular oxygenation results in a change in tissue oxygenation in a model that is responsive to a hyperoxic challenge

We looked for the impact of the change in tumor vascular oxygenation on the tissue oxygenation. For this purpose, we tested correlations between ΔR_2^* and ΔR_{1L}, ΔR_{1W} and ΔR_{1G} of the same tumors.

A more negative ΔR_2^* corresponds to a better reoxygenation of the vascular compartment in response to CB, whereas a more positive ΔR_1 corresponds to a better reoxygenation of the tissue compartment.

In rhabdomyosarcomas, correlations of ΔR_{1W} and ΔR_2^*, and ΔR_{1L} and ΔR_2^*, were significant (Figure 2B: ΔR_{1W} and ΔR_2^*, $p = 0.02$, $r = -0.50$; Figure 2C: ΔR_{1L} and ΔR_2^*, $p < 0.01$, $r = -0.63$). However, the correlation of ΔR_{1G} and ΔR_2^* was not significant, although a trend was present (Figure 2A, $p = 0.07$, $r = -0.40$). In this tumor model, the vascular reoxygenation in response to CB challenge led to a significant change in tissue oxygenation.[24]

However, similar analysis in the 9L–glioma model, which shows a higher basal oxygenation,[24] did not give any significant correlation between vascular and tissue changes in oxygenation (Figure 2D–F).

Interestingly, correlations of the pooled data of the two tumor models were stronger than the correlations of each model separately (Figure 2G: ΔR_{1G} and ΔR_2^*, $p = 0.01$, $r = -0.40$; Figure 2H: ΔR_{1W} and ΔR_2^*, $p = 0.03$, $r = -0.35$; Figure 2I: ΔR_{1L} and ΔR_2^*, $p < 0.01$, $r = -0.49$).

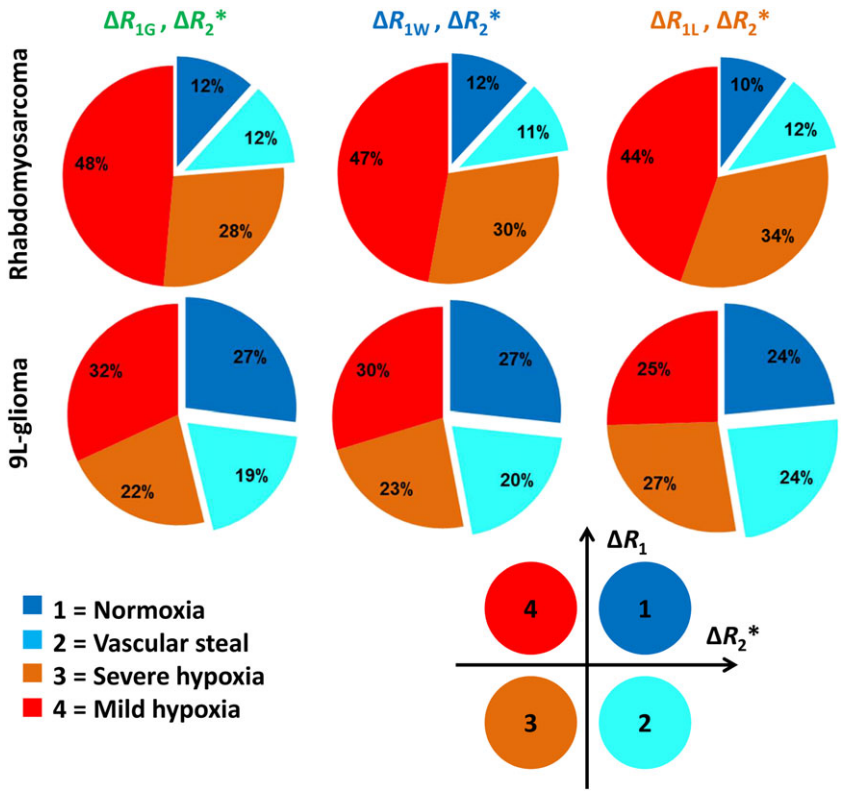

FIGURE 4 Mean fractional carbogen-induced ΔR_1, ΔR_2^* response categories from rhabdomyosarcomas (top row) and 9L–gliomas (bottom row) showing the percentage of total region of interest (ROI) voxels. Each tumor is fractionated based on the response of ΔR_1 and ΔR_2^* to carbogen challenge of each voxel (see graph at the bottom right). From left to right: ΔR_{1G} and ΔR_2^*, ΔR_{1W} and ΔR_2^*, and ΔR_{1L} and ΔR_2^* analyses

TABLE 1 Heterogeneity of response of R_1 and R_2^* to carbogen challenge. Each voxel was encoded by a different color depending on its carbogen-induced ΔR_1 and ΔR_2^*. Blue indicates voxels with $\Delta R_1 > 0$ and $\Delta R_2^* \geq 0$, cyan voxels with $\Delta R_2^* > 0$ and $\Delta R_1 < 0$, orange voxels with $\Delta R_1 \leq 0$ and $\Delta R_2^* < 0$ and red voxels with $\Delta R_1 > 0$ and $\Delta R_2^* < 0$

Response category	% total ROI voxels (ΔR_{1G} and ΔR_2^*)			% total ROI voxels (ΔR_{1W} and ΔR_2^*)			% total ROI voxels (ΔR_{1L} and ΔR_2^*)		
	9L–glioma	Rhabdomyosarcoma	p	9L–glioma	Rhabdomyosarcoma	p	9L–glioma	Rhabdomyosarcoma	p
Blue	27.0 ± 2.8	11.7 ± 2.0	<0.0001	26.7 ± 2.0	11.9 ± 1.4	<0.0001	23.6 ± 2.0	10.1 ± 1.4	<0.0001
Cyan	19.2 ± 2.3	12.1 ± 3.0	*0.0713*	20.3 ± 1.1	10.6 ± 2.3	0.0010	23.8 ± 1.4	11.6 ± 2.6	0.0005
Orange	21.9 ± 2.8	27.7 ± 3.3	*0.1997*	23.3 ± 1.8	30.4 ± 1.7	0.0066	27.2 ± 2.0	33.7 ± 1.9	0.0238
Red	31.9 ± 3.1	48.6 ± 5.2	0.0120	29.7 ± 1.7	47.1 ± 3.4	0.0001	25.5 ± 1.7	44.6 ± 3.6	<0.0001
Orange–red	53.8 ± 2.6	76.2 ± 3.9	<0.0001	53.0 ± 2.6	77.5 ± 3.4	<0.0001	49.8 ± 4.0	78.3 ± 3.8	<0.0001

Values are mean ± standard error of the mean (SEM); unpaired *t*-test. The significance of italic 'p' values marked the $p > 0.05$.

3.3 | In the tissue compartment, the basal tumor oxygenation does not influence the response to a hyperoxic challenge

As rhabdomyosarcoma and 9L–glioma exhibit different basal oxygenation status (rhabdomyosarcoma being more hypoxic than 9L–glioma[24]), we sought a possible impact of the basal oxygenation status on the amplitude of response in tumor tissues to the hyperoxic challenge. Faster median R_1 values correspond to a better tissue oxygenation, and a positive ΔR_1 corresponds to a better reoxygenation of the tissue compartment in response to CB. We tested correlations between R_{1G}, R_{1W} and R_{1L} and their corresponding delta values (R_{1G} and ΔR_{1G}, R_{1W} and ΔR_{1W}, R_{1L} and ΔR_{1L}) in both tumor models.

Except for a weak correlation between R_{1W} and ΔR_{1W} in rhabdomyosarcoma ($p = 0.05$, $r = 0.43$; Figure 3A), the remaining correlations of rhabdomyosarcoma and 9L–glioma were insignificant (Figure 3A). It should be noted that the basal R_1 of 9L–gliomas (2.26 ± 0.03 s^{-1}) is significantly higher than the basal R_1 of rhabdomyosarcomas (2.16 ± 0.03 s^{-1}) ($p = 0.02$). Although correlations of median values of R_{1G} and ΔR_{1G}, R_{1W} and ΔR_{1W}, and R_{1L} and ΔR_{1L} show that a relation between the basal tissue oxygenation and its response to CB does not exist, the representative maps of basal R_{1G} and ΔR_{1G} of a rhabdomyosarcoma (Figure 3B) suggest the contrary. Indeed, the region which is initially better oxygenated (hotter color, R_{1G} basal map) appears to be more responsive to CB challenge (hotter color, ΔR_{1G} map), and vice versa. The correlation between R_{1G} and ΔR_{1G} of voxels within this tumor was significant ($p < 0.01$, $r = 0.16$, Supporting Information Figure S3). This observation underlines the importance of the tumor heterogeneity and suggests that further analysis at the voxel scale should be considered. Therefore, a multi-parametric intra-tumoral analysis was performed.

3.4 | Multi-parametric analysis of tumor heterogeneity of response to a hyperoxic challenge

The multi-parametric analysis was performed by superimposing the two maps of ΔR_{1G} and ΔR_2^*, ΔR_{1W} and ΔR_2^*, and ΔR_{1L} and ΔR_2^* voxel by voxel. Each voxel was encoded by different colors depending on its CB-induced ΔR_1, ΔR_2^* as shown in Figure 4.

In order to quantify the distribution of the four fractions, the percentage of tumor voxels of each color code was calculated (Figure 4). In the analysis of ΔR_2^* and ΔR_{1G}, ΔR_2^* and ΔR_{1W}, and ΔR_2^* and ΔR_{1L} in the two models, the percentage of 'blue voxels' was significantly higher in 9L–gliomas, whereas the percentage of 'red voxels' was significantly higher in rhabdomyosarcomas (Table 1). In the analysis of ΔR_2^* and ΔR_{1G}, we observed a higher percentage of 'cyan voxels' in 9L–glioma than in rhabdomyosarcoma, but the difference was insignificant ($p = 0.07$). Meanwhile, there was no significant difference between the percentage of 'orange voxels' ($p = 0.20$) between the two models. The same analysis using ΔR_{1W} and ΔR_{1L} with ΔR_2^* showed a significantly higher proportion of 'cyan voxels' in 9L–glioma and a significantly higher proportion of 'orange voxels' in rhabdomyosarcoma. These observations indicate that the multi-parametric analysis of tumor response to hyperoxic breathing challlenge could be useful to characterize the tumor oxygenation heterogeneity.

3.5 | Total lipid content

No significant difference was found between the lipid contents in the two tumor models: 2.1 ± 0.1% and 2.3 ± 0.2% for rhabdomyosarcomas and 9L–gliomas, respectively (mean ± SEM).

3.6 | α-SMA staining

The α-SMA-positive area percentages were 5.7 ± 0.5% and 1.9 ± 0.2% for rhabdomyosarcomas and 9L–gliomas, respectively ($p < 0.01$, unpaired *t*-test).

4 | DISCUSSION

In this study, CB was used to alter tumor oxygenation. This gas increases the oxygen supply to the tumor by saturation of the arterial blood. Other possible impacts of CB are as follows: (1) an increase in the rate of breathing; (2) a decrease in the blood pH, resulting in an increase in O_2 delivery by right shifting of the dissociation curve of hemoglobin and O_2; (3) counteraction of the vasoconstriction effect of O_2 by the CO_2 component.[25] In the two models studied, CB induced a greater effect in tumors that were initially less oxygenated in the vascular compartment (faster basal R_2^* values; Figure 1). Indeed, in these tumors, dHb was more abundant at baseline status and these free heme sites of dHb preferentially bind to oxygen under the hyperoxic breathing CB challenge. In contrast, a high proportion of hemoglobin was already saturated at baseline status in tumors with a well-oxygenated vascular compartment. Thus, the hyperoxic challenge barely changed the amount of dHb in these tumors.[21] This observation is in agreement with a previous study which showed that R_2^* was more sensitive in a situation of low oxygenation.[26] This observation held true at both the inter- and intra-tumoral levels (Figure 1), as well as between models. It should be noted that CB induced a significantly greater reduction in R_2^* in rhabdomyosarcomas than in 9L–gliomas ($p < 0.01$, unpaired Student's *t*-test, Supporting Information Figure S4). Meanwhile, 9L–gliomas have been described to present a better basal oxygenation status than rhabdomyosarcomas.[24] In conclusion, in this context, CB could modulate the vascular oxygenation in the two tumor models studied, and the magnitude of modification was dependent on the basal tumor oxygenation status.

It should be noted that, in the case of 13762NF breast carcinoma,[27] the change in R_2^* induced by oxygen challenge was not found to be correlated with the baseline R_2^* value in a voxel-by-voxel analysis. This behavior may contradict the results observed in the present study (Figure 1). However, different levels of tumor oxygenation between models could contribute to this observation. Indeed, the 13762NF carcinomas studied in the work of Zhao et al.[27] were better oxygenated than the 9L–gliomas and rhabdomyosarcomas in the current work. Under oxygen breathing, pO_2 of 13762NF increased from 18 to 68 Torr. However, pO_2 increased from 9 to 17 mmHg and 5 to 9 mmHg under CB breathing in 9L–gliomas and rhabdomyosarcomas, respectively.[24] As stated in the work of Baudelet and Gallez,[26] the *in vivo* blood oxygenation level-dependent (BOLD) signal change was more pronounced when passing from 5 to 15 mmHg than the higher range of pO_2, and a plateau was reached at a pO_2 value above 30 mmHg. Thus, the lack of correlation between R_2^* and oxygen-induced ΔR_2^* in 13762NF carcinomas could be a result of the lack of ΔR_2^* change because of the abundance of well-oxygenated voxels. Hence, only a slight change in ΔR_2^* occurred when these voxels reached a superior level of oxygenation.

It was expected that tumors which had benefited from vascular reoxygenation induced by CB would also show an increase in oxygenation in the tissue compartment. This behavior was seen in the more hypoxic rhabdomyosarcoma tumor model ($p < 0.05$), but a lack of correlation was found in the 9L–glioma model (Figure 2). Remarkably, the correlations of the pooled data (Figure 2G–I) were stronger than the correlations of each model separately (Figure 2A–C for rhabdomyosarcomas and Figure 2D–F for 9L–gliomas). This observation was consistent with an increase in vascular oxygenation generating an elevated tumor pO_2 and could be explained as follows. First, the mechanism of CB for the modification of tumor oxygenation is to increase the O_2 supply. Second, both 9L–glioma and rhabdomyosarcoma models have been demonstrated previously to be responsive to CB breathing.[24]

Interestingly, the correlation of the R_1 and R_2^* responses to CB challenge of Dunning prostate R3327-HI and R3327-AT1 tumors[20] reveals a remarkably similar behavior to Figure 2. Indeed, in both studies, one model showed a significant correlation between ΔR_1 and ΔR_2^* (HI and rhabdomyosarcomas), whereas the other showed no relation (AT1 and 9L–gliomas). It should be noted that HI tumors are known to be better vascularized and less hypoxic than AT1 tumors. However, rhabdomyosarcomas have been reported to be more hypoxic than 9L–gliomas. Although this seems to be controversial as the correlation was observed in a less hypoxic model (HI compared with AT1) and a more hypoxic model (rhabdomyosarcoma compared with 9L–glioma), we all noted a poor response of R_2^* in AT1 and 9L–gliomas. In brief, whether the small ΔR_2^* originates from the poor vascularization or from saturated dHb, it could be the reason for the lack of correlation between ΔR_1 and ΔR_2^*.

Another scenario was seen in the work of Burrell et al.,[21] where R_1 and R_2^* were measured pre- and post-CB breathing in GH3 and PC3 tumors. The scatter plot showing the relationship between ΔR_1 and ΔR_2^* suggested that a smaller ΔR_2^* was associated with a larger ΔR_1, and vice versa, but no significant relationship was found. GH3 has been reported to be more hypoxic than PC3. The authors theorized that there was a high proportion of dHb in the blood of the hypoxic GH3 model. Hence, the elevated O_2 supplied by CB leads to a decrease in the dHb content of the tumor, and thus a decrease in R_2^*. Meanwhile, in the less hypoxic model PC3, where dHb was already saturated, a boost in O_2 supply did not change the dHb content, but resulted in an increase in dissolved O_2, and thus increased R_1. The hypothesis was supported by a faster R_2^* baseline and a slower R_1 baseline of GH3 than of PC3, which suggested a richer dHb content in GH3 and a higher pO_2 in PC3. Moreover, the CB-induced ΔR_2^* in GH3 was significantly larger than that in PC3, which is consistent with this hypothesis. Although no significant difference between ΔR_1 of GH3 and PC3 was reported, the authors observed a larger change in PC3. In brief, the lack of correlation of ΔR_1 and ΔR_2^* could be a result of the lack of ΔR_1 change in GH3 and the lack of ΔR_2^* change in PC3.

With regard to the translational aspect, Remmele et al.[22] used combined R_1 and R_2^* parameters to study human brain tumors. They established a voxel-wise scatter plot (CB-induced ΔR_1 and ΔR_2^*) of different areas in the brain. The shape and distribution of the cluster provided information on the change in dHb and O_2 content, and thus served as a tool to classify tissue regions.

The magnitude of the response of ΔR_1 to CB could not be correlated with its basal status in the tumor models in this study (Figure 3A, except for a weak correlation of ΔR_{1W}–R_{1W} in rhabdomyosarcoma). The representative maps of R_{1G} and ΔR_{1G} of a rhabdomyosarcoma, however, suggest that there may be a relationship between basal R_1 and its response to CB at the intra-tumoral level. Therefore, an intra-tumoral analysis was performed which revealed four different types of voxel behavior, based on the response to CB in terms of ΔR_1 and ΔR_2^*.

In the so-called 'red voxels', CB induced an increase in R_1 and a decrease in R_2^*, which means an increase in dissolved oxygen and a decrease in [dHb]. Mild hypoxia is a reasonable hypothesis for this type of voxel. Indeed, to obtain this type of response, hemoglobin should not be completely saturated at baseline status. As the hyperoxic challenge is induced, increasing oxygen would bind to the heme sites of the free dHb molecules,

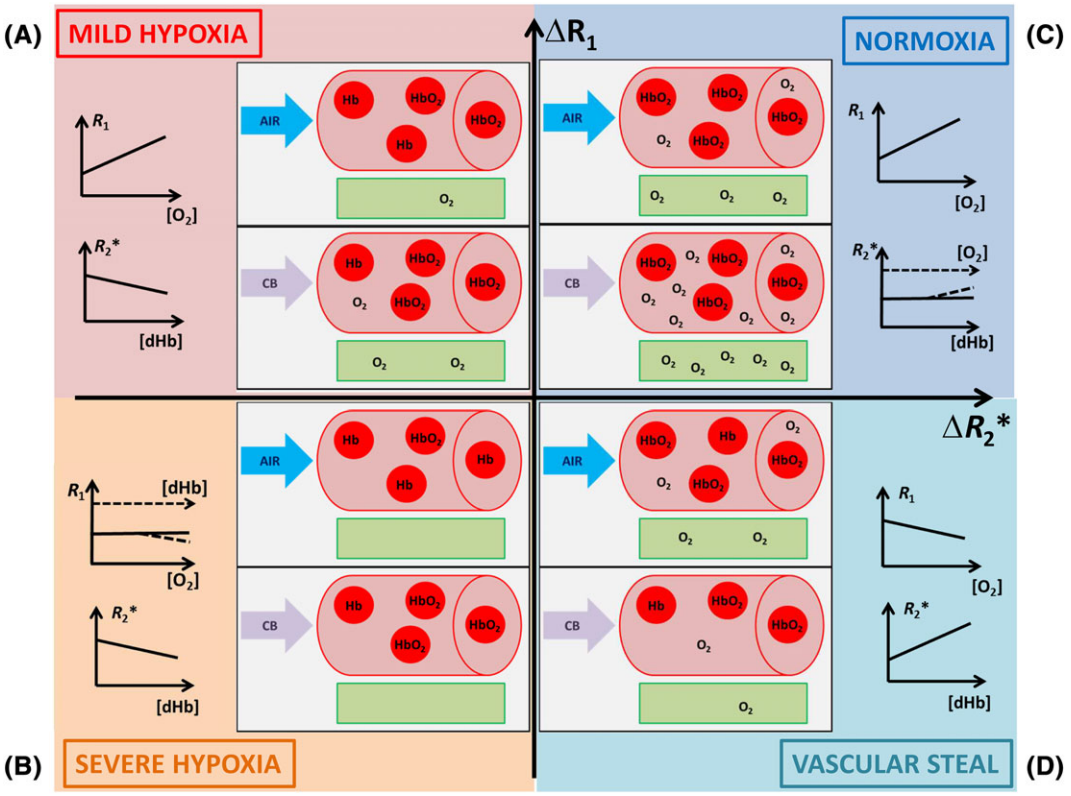

FIGURE 5 Hypothesis corresponding to red (A), orange (B), blue (C) and cyan (D) voxels. The arrows indicate the breathing conditions applied [blue arrow, air; purple arrow, carbogen (CB)]. The red cylinder is the vessel and the green box is the tumor tissue. The red blood cells are represented by red spheres. dHb, deoxyhemoglobin; Hb, hemoglobin

thereby decreasing [dHb], and thus decreasing R_2*. The remaining oxygen re-oxygenates the tissue, which increases the content of dissolved oxygen, thus increasing R_1 (Figure 5A).

In a more severely hypoxic tissue, represented by 'orange voxels' ($\Delta R_1 \leq 0$ and $\Delta R_2^* < 0$, Figure 5B), the majority of hemoglobin should be unsaturated at baseline. The extra oxygen supply brought by the CB challenge is just enough to bind to dHb, but hardly able to increase the amount of dissolved oxygen. Thus, R_2* decreases as the result of a decrease in [dHb]. Interestingly, R_1 does not exclusively depend on the concentration of dissolved oxygen, but also on the paramagnetic [dHb].[28] At a low hemoglobin saturation level, an increase in O_2 supply decreases R_1 as a result of the decrease in [dHb]. The value of R_1 is minimal when all the heme sites are bound to oxygen and dissolved oxygen is minimal.[28] Severe hypoxia could be a possible explanation for the 'orange voxels' in which $\Delta R_1 > 0$ is absent. This theory is in agreement with the work of O'Connor et al.[23]

In the opposite case of the so-called 'blue voxels', where $R_1 > 0$ and $R_2^* \geq 0$, we attribute these voxels to normoxic tissue (Figure 5C). In this tissue type, most of the hemoglobin molecules are already saturated, which hinders further oxygen binding when hyperoxygenation is induced. Thus, the CB challenge increases only the concentration of dissolved oxygen and the dHb/HbO_2 ratio remains almost constant. Consequently, $\Delta R_1 > 0$ is observed. As R_2* is sensitive to [dHb], it depends on the blood oxygen saturation, hematocrit and the blood volume.[10]

In this context, using CB, a change in hematocrit was not expected. There are therefore two possible schemes for the increase in R_2*.

1. $\Delta R_2^* > 0$ could be caused by the change in dissolved oxygen in the blood compartment. There are two mechanisms explaining the effect of oxygen on R_2*.[29] First, the increase in paramagnetic oxygen influences the magnetic susceptibility difference between blood and tissue. Second, $\Delta R_2^* > 0$ is indirectly linked to the oxygen–hemoglobin dissociation curve. In tissues that are normoxic at baseline, most of the oxygen molecules are bound to hemoglobin. During capillary transit, oxygen is extracted from the heme sites. Thus, there is a dramatic decrease in oxygen–hemoglobin. Under a CB challenge, the concentration of bound oxygen remains almost unchanged compared with baseline with a significant increase in dissolved oxygen. The capillary transit extracts preferably the unbound oxygen and leaves the oxygen bound to hemoglobin nearly untouched. Hence, $\Delta R_2^* > 0$ is the result of the increase in [dHb] at baseline.
2. The increase in R_2* could also be linked to the increase in regional blood volume. The tumor vasculature comprises both mature and unstable, immature blood vessels. Only the mature blood vessels with the pericytes integrated in the wall are believed to be 'responsive' to CB breathing. In other words, the mature blood vessels could be dilated under the effect of the CO_2 component of CB, thereby inducing an increase in blood volume in the neighborhood and a steal effect in other parts of the tumor. The increase in blood volume leads to an increase in [dHb] in an image voxel. It should be noted that the increase in blood volume and the increase in blood oxygenation have inverse effects on R_2*.[10] A similar response, where hyperoxic challenge increases R_2*, has been observed in normal tissue.[16]

Interestingly, the surface of pericyte coverage detected by immunohistochemistry was significantly higher in rhabdomyosarcomas than in 9L–gliomas. In other words, the blood volume effect of R_2* might be more remarkable in rhabdomyosarcomas than in 9L–gliomas (scheme 2). However, the proportion of blue voxels in rhabdomyosarcomas was significantly smaller than that in 9L–gliomas. This observation supports the first scheme (scheme 1) proposing that the increase in R_2* is predominantly a result of the change in dissolved oxygen in the blood compartment.

The last voxel behavior in response to CB is represented by 'cyan voxels' ($\Delta R_1 < 0$ and $\Delta R_2^* > 0$, Figure 5D). This type of response could be a result of the vascular steal effect. Indeed, the CO_2 component of CB is believed to have a vasodilation effect on mature blood vessels.[30] Meanwhile, the tumor vasculature is heterogeneous, and is composed of mature and immature vessels (which do not respond to CO_2).[30] Hence, under CB challenge, the dilated mature vessels redistribute the blood away from sites of immature vessels. This event leads to further blood desaturation (i.e. increased dHb/HbO_2 ratio) and a decreased oxygen concentration. Thus, a decrease in R_1 and an increase in R_2* are observed. Previous studies on the steal effect of the whole tumor induced by hydralazine have provided a similar trend of R_1 and R_2* responses.[23,31]

Briefly, based on the hypothesis of four types of voxel, 9L–gliomas present more normoxic fractions than rhabdomyosarcomas (Table 1, blue voxels). Furthermore, about three-quarters of rhabdomyosarcomas *versus* one-half of 9L–gliomas were found to be hypoxic (both severe hypoxia and mild hypoxia; Table 1, orange and red voxels). This observation is in accordance with that observed in the work of Tran et al.[24] using EPR oximetry and ^{18}F–FAZA positron emission tomography.

In line with the work of O'Connor et al.,[23] we confirm that the median values of ΔR_1 and ΔR_2^* are not robust enough to represent the tumor oxygenation status quantitatively, or the extent of hypoxia, which emphasizes the importance of the intra-tumoral heterogeneity.

In the current work, R_{1L} and R_{1W} values deconvoluted from R_{1G} showed no advantage in terms of the predictive capacity of the basal tumor oxygenation or of the response of tumor to CB breathing, except in the correlations between ΔR_1 and ΔR_2^* in the rhabdomyosarcoma tumor model (Figure 2A–C). Indeed, although ΔR_{1G} and ΔR_2^* correlation was unable to show an impact of vascular reoxygenation on the change in tissue oxygenation ($p = 0.07$, Figure 2A), correlations of ΔR_2^*, ΔR_{1L} and ΔR_2^*, ΔR_{1W} were significant (Figure 2B: ΔR_{1W} and ΔR_2^*, $p = 0.02$; Figure 2C: ΔR_{1L} and ΔR_2^*, $p < 0.01$).

The major contribution of this work is to provide a concept to map tumor oxygenation by combining different endogenous oxygen-sensitive markers. Indeed, this is a noninvasive, easily translatable method to broaden the understanding and assessment of tumor oxygenation, as there is currently no gold standard to measure hypoxia. Moreover, this work addresses tumor heterogeneity by analyzing changes in the relaxation parameters at the voxel scale. Thus, the segmentation of tumor voxels with respect to their type of response to a hyperoxic challenge could be useful to predict tumor hypoxia, and could be translated and evaluated in other tumor models as well as in the clinical setting.

4.1 | Limitations

The use of CB to alter tumor hypoxia could induce some changes that might become potential sources of R_1 and R_2^* fluctuations. CB could induce a vasodilation effect on mature blood vessels. This could create a change in blood flow that influences R_1[12] and/or a change in blood volume that alters [dHb] per tissue volume, thereby influencing R_2^*.[10] In addition, CB could induce blood acidification which, in turn, might shift the O_2–hemoglobin dissociation curve to the right. This effect might increase R_2^*.[10] It should be noted that the right shift of the hemoglobin–O_2 dissociation curve and the blood volume induce a potential increase in R_2^*, whereas blood oxygenation decreases R_2^*.

It should be noted that tumors often show spontaneous fluctuations in O_2. In FSa fibrosarcomas, the spontaneous fluctuations in T_2^* were proven to be associated with the fluctuations in tumor oxygenation linked to acute hypoxia, which occurs both in functional tumor regions and in tumor regions with non-perfused and/or immature vessels.[32,33] It would be ideal to assess the average of several maps pre- and post-challenge or to increase the imaging time, as a longer time could reveal regions exhibiting a longer cycle of hypoxia.[32] The authors discovered that the frequency of the fluctuation cycle ranged from 3 min to 1 h.[32] In the current work, the acquisition times of R_1 and R_2^* were 20 and 10 min, respectively. This acquisition time could cover at least the short fluctuation cycles.

ACKNOWLEDGEMENTS

This study was supported by grants from the Belgian National Fund for Scientific Research (FNRS) and the 'Fournier-Majoie Foundation'.

ORCID

Bernard Gallez http://orcid.org/0000-0002-5708-1302
Bénédicte F. Jordan http://orcid.org/0000-0002-7126-2206

REFERENCES

1. Overgaard J. Hypoxic radiosensitization: adored and ignored. *J Clin Oncol*. 2007;25:4066-4074.
2. Dewhirst MW, Birer SR. Oxygen-enhanced MRI is a major advance in tumor hypoxia imaging. *Cancer Res*. 2016;76:769-772.
3. Krohn KA, Link JM, Mason RP. Molecular imaging of hypoxia. *J Nucl Med*. 2008;49(Suppl. 2):129S-148S.
4. Tatum JL. Hypoxia: importance in tumor biology, noninvasive measurement by imaging, and value of its measurement in the management of cancer therapy. *Int J Radiat Biol*. 2006;82:699-757.
5. Jordan BF, Cron GO, Gallez B. Rapid monitoring of oxygenation by ^{19}F magnetic resonance imaging: simultaneous comparison with fluorescence quenching. *Magn Reson Med*. 2009;61:634-638.
6. Gallez B, Baudelet C, Jordan BF. Assessment of tumor oxygenation by electron paramagnetic resonance: principles and applications. *NMR Biomed*. 2004;17:240-262.
7. Kodibagkar VD, Wang X, Pacheco-Torres J, Gulaka P, Mason RP. Proton imaging of siloxanes to map tissue oxygenation levels (PISTOL): a tool for quantitative tissue oximetry. *NMR Biomed*. 2008;21:899-907.
8. Dewhirst MW, Klitzman B, Braun RD, Brizel DM, Haroon ZA, Secomb TW. Review of methods used to study oxygen transport at the microcirculatory level. *Int J Cancer*. 2000;90:237-255.
9. Gu Y, Bourke VA, Kim JG, Constantinescu A, Mason RP, Liu H. Dynamic response of breast tumor oxygenation to hyperoxic respiratory challenge monitored with three oxygen-sensitive parameters. *Appl Optics*. 2003;42:2960-2967.
10. Baudelet C, Gallez B. Current issues in the utility of blood oxygen level dependent MRI for the assessment of modulations in tumor oxygenation. *Curr Med Imag Rev*. 2005;1:229-243.
11. Mürtz P, Flacke S, Müller A, et al. Changes in the MR relaxation rate R_2^* induced by respiratory challenges at 3.0 T: a comparison of two quantification methods. *NMR Biomed*. 2010;23:1053-1060.
12. O'Connor JPB, Naish JH, Parker GJM, et al. Preliminary study of oxygen-enhanced longitudinal relaxation in MRI: a potential novel biomarker of oxygenation changes in solid tumors. *Int J Radiat Oncol Biol Phys*. 2009;75:1209-1215.
13. Jordan BF, Magat J, Colliez F, et al. Mapping of oxygen by imaging lipids relaxation enhancement: a potential sensitive endogenous MRI contrast to map variations in tissue oxygenation. *Magn Reson Med*. 2013;70:732-744.
14. Colliez F, Neveu MA, Magat J, Cao-Pham TT, Gallez B, Jordan BF. Qualification of a noninvasive magnetic resonance imaging biomarker to assess tumor oxygenation. *Clin Cancer Res*. 2014;20:5403-5411.
15. Cao-Pham T-T, Tran L-B-A, Colliez F, et al. Monitoring tumor response to carbogen breathing by oxygen-sensitive magnetic resonance parameters to predict the outcome of radiation therapy: a preclinical study. *Int J Radiat Oncol Biol Phys*. 2016;96:149-160.
16. O'Connor JPB, Naish JH, Jackson A, et al. Comparison of normal tissue R_1 and R_2^* modulation by oxygen and carbogen. *Magn Reson Med*. 2009;61:75-83.
17. White DA, Zhang Z, Li L, et al. Developing oxygen-enhanced magnetic resonance imaging as a prognostic biomarker of radiation response. *Cancer Lett*. 2016;380:69-77.
18. Winter JD, Akens MK, Cheng H-LM. Quantitative MRI assessment of VX2 tumour oxygenation changes in response to hyperoxia and hypercapnia. *Phys Med Biol*. 2011;56:1225.
19. Hallac RR, Zhou H, Pidikiti R, et al. Correlations of noninvasive BOLD and TOLD MRI with pO2 and relevance to tumor radiation response. *Magn Reson Med*. 2014;71:1863-1873.
20. Zhao D, Pacheco-Torres J, Hallac RR, et al. Dynamic oxygen challenge evaluated by NMR T_1 and T_2^*-insights into tumor oxygenation. *NMR Biomed*. 2015;28:937-947.

21. Burrell JS, Walker-Samuel S, Baker LCJ, et al. Exploring ΔR_2^* and ΔR_1 as imaging biomarkers of tumor oxygenation. *J Magn Reson Imaging*. 2013;38:429-434.
22. Remmele S, Sprinkart AM, Müller A, et al. Dynamic and simultaneous MR measurement of R_1 and R_2^* changes during respiratory challenges for the assessment of blood and tissue oxygenation. *Magn Reson Med*. 2013;70:136-146.
23. O'Connor JPB, Boult JKR, Jamin Y, et al. Oxygen-enhanced MRI accurately identifies, quantifies, and maps tumor hypoxia in preclinical cancer models. *Cancer Res*. 2016;76:787-795.
24. Tran LBA, Bol A, Labar D, et al. Potential role of hypoxia imaging using ^{18}F-FAZA PET to guide hypoxia-driven interventions (carbogen breathing or dose escalation) in radiation therapy. *Radiother Oncol*. 2014;113:204-209.
25. Kaanders JH, Bussink J, van der Kogel AJ. ARCON: a novel biology-based approach in radiotherapy. *Lancet Oncol*. 2002;3:728-737.
26. Baudelet C, Gallez B. How does blood oxygen level-dependent (BOLD) contrast correlate with oxygen partial pressure (pO_2) inside tumors? *Magn Reson Med*. 2002;48:980-986.
27. Zhao D, Jiang L, Hahn EW, Mason RP. Comparison of ^{1}H blood oxygen level-dependent (BOLD) and ^{19}F MRI to investigate tumor oxygenation. *Magn Reson Med*. 2009;62:357-364.
28. Blockley NP, Jiang L, Gardener AG, Ludman CN, Francis ST, Gowland PA. Field strength dependence of R_1 and R_2^* relaxivities of human whole blood to prohance, vasovist, and deoxyhemoglobin. *Magn Reson Med*. 2008;60:1313-1320.
29. Schwarzbauer C, Deichmann R. Vascular component analysis of hyperoxic and hypercapnic BOLD contrast. *Neuroimage*. 2012;59:2401-2412.
30. Robinson SP, Rijken PFJW, Howe FA, et al. Tumor vascular architecture and function evaluated by non-invasive susceptibility MRI methods and immunohistochemistry. *J Magn Reson Imaging*. 2003;17:445-454.
31. Howe FA, Robinson SP, McIntyre DJO, Stubbs M, Griffiths JR. Issues in flow and oxygenation dependent contrast (FLOOD) imaging of tumours. *NMR Biomed*. 2001;14:497-506.
32. Baudelet C, Ansiaux R, Jordan BF, Havaux X, Macq B, Gallez B. Physiological noise in murine solid tumours using T_2^*-weighted gradient-echo imaging: a marker of tumour acute hypoxia? *Phys Med Biol*. 2004;49:3389-3411.
33. Baudelet C, Cron GO, Ansiaux R, et al. The role of vessel maturation and vessel functionality in spontaneous fluctuations of T_2^*-weighted GRE signal within tumors. *NMR Biomed*. 2006;19:69-76.

SUPPORTING INFORMATION

Additional Supporting Information may be found online in the supporting information tab for this article.

How to cite this article: Cao-Pham T-T, Joudiou N, Van Hul M, et al. Combined endogenous MR biomarkers to predict basal tumor oxygenation and response to hyperoxic challenge. *NMR in Biomedicine*. 2017;30:e3836. https://doi.org/10.1002/nbm.3836